Insight into the Sealing Capacity of Mudrocks determined using a Digital Rock Physics Workflow

TACCSTER 2019

Abhishek Bihani[1], Hugh Daigle[1], Javier E. Santos[1], Christopher Landry[2], Maša Prodanović[1], Kitty Milliken[2]

[1]Hildebrand Department of Petroleum and Geosystems Engineering, University of Texas at Austin.

[2]Bureau of Economic Geology, University of Texas at Austin, Austin, Texas, USA.

Abstract

Primary objective: To better understand seal capacity in mudrocks and to determine the conditions under which a mudrock seal fails by allowing a non-wetting fluid to percolate.

Hypothesis: Mudrock seals can fail below the fracture pressure if there exists a percolating pathway formed due to a continuous and sufficiently large pore-throat system.

Procedure: We used SEM images of uncemented muds obtained at various depths (< 1.1 km burial) in the Kumano Basin offshore Japan for the study. Image mosaics were filtered and segmented using conventional and machine-learning techniques to identify the pore space, silt, and clay grains. We applied a 3D stochastic technique for pore space reconstruction from the SEM images and simulated capillary drainage in the resulting 3D volumes by the lattice Boltzmann method (LBM) using Stampede 2.

Conclusion: Results showed that porosity and permeability decreased with depth, and capillary threshold pressure values increased. However, increasing silt content at a particular depth counteracted this behavior, due to better preservation of larger pores and throats.

Sealing capacity of mudrocks

- Failure modes of a seal:

a) Darcy flow b) Flow through faults/fractures c) Diffusion

- Washburn Equation: $P_c = \frac{2\sigma \cos\theta}{r}$

where P_c is capillary pressure, σ is interfacial tension, θ is contact angle and r is throat radius

- Mudrock seals have nanometer-scale pore throats with high capillary pressures

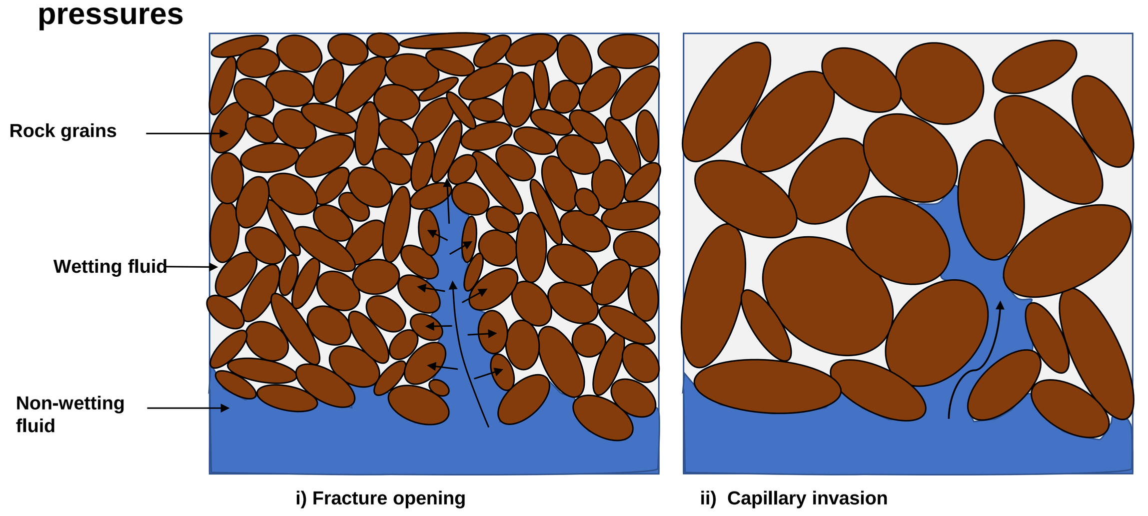

Figure 1 - Effect of buoyant pressure and grain size: i) fracturing, ii) capillary invasion

Silt bridging in mudrocks

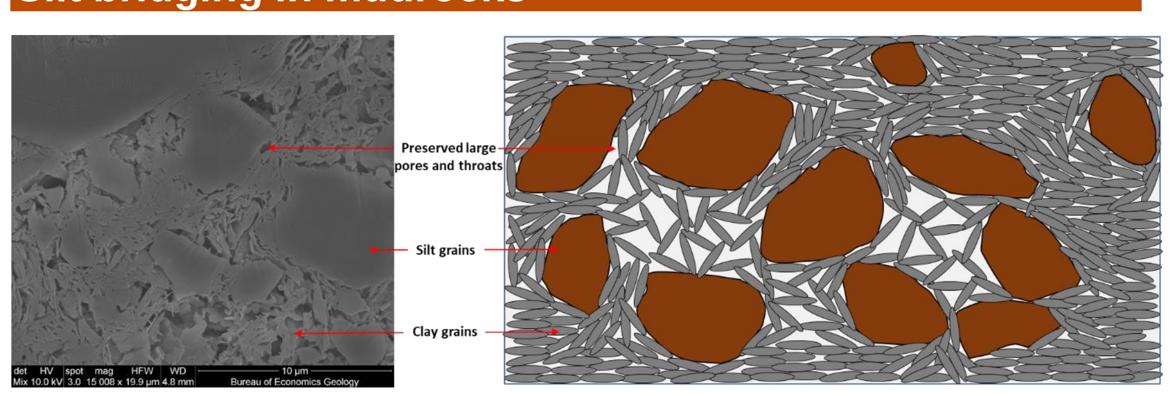

Figure 2- A) An SEM image at a depth of 202 mbsf (Milliken et al., 2016), B) Silt bridging in mudrocks (Modified from Schneider et al., 2011).

- Dual porosity is formed in mudrocks due to silt-bridging

1. Silt bridging preserves large pore throats
2. Stress bridges inhibit clay particle alignment

- Silt bridging effect increases vertical permeability and lowers threshold pressure in mudrock (Bihani and Daigle, 2019).

SEM images from Kumano Basin

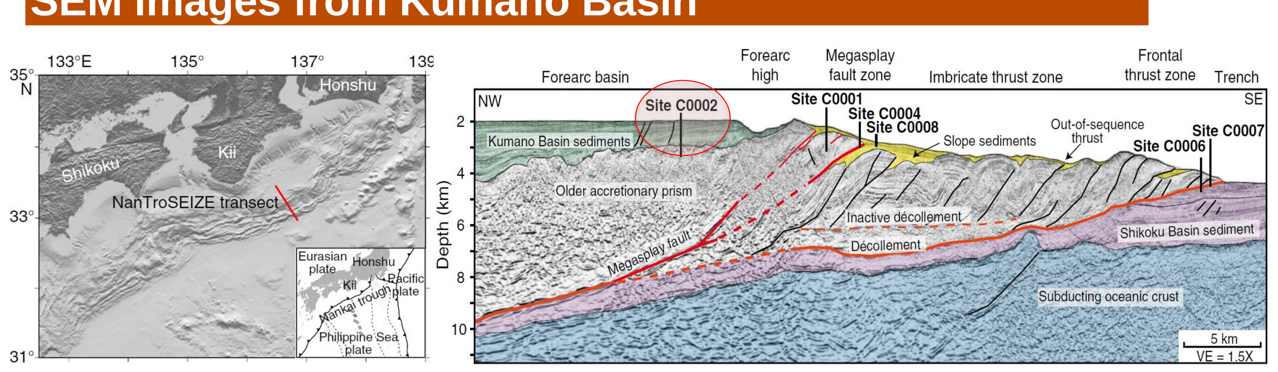

Figure 3- Nankai Trough: location and interpreted seismic section (modified from Kopf et al., 2011)

Sample source (core and length)	Top depth (meters below sea floor- mbsf)	Unit	Number of images
C0002D-3H-3, 119.0-121.0 cm	19.15	I	5
C0002D-18H-4, 11.0-13.0 cm	202.15	I	10
C0002L-14X-1 W, 102.0-103.0 cm	401.52	II	10
C0002B-10R-3, 48.0-50.0 cm	600.62	II	13
C0002B-40R-3, 45.0-48.0 cm	836.28	III	11

Table 1- Details of SEM images obtained at site C0002 used for analysis

Image analysis: filtering and segmentation

- All the images were processed to identify individual pores and silt grains

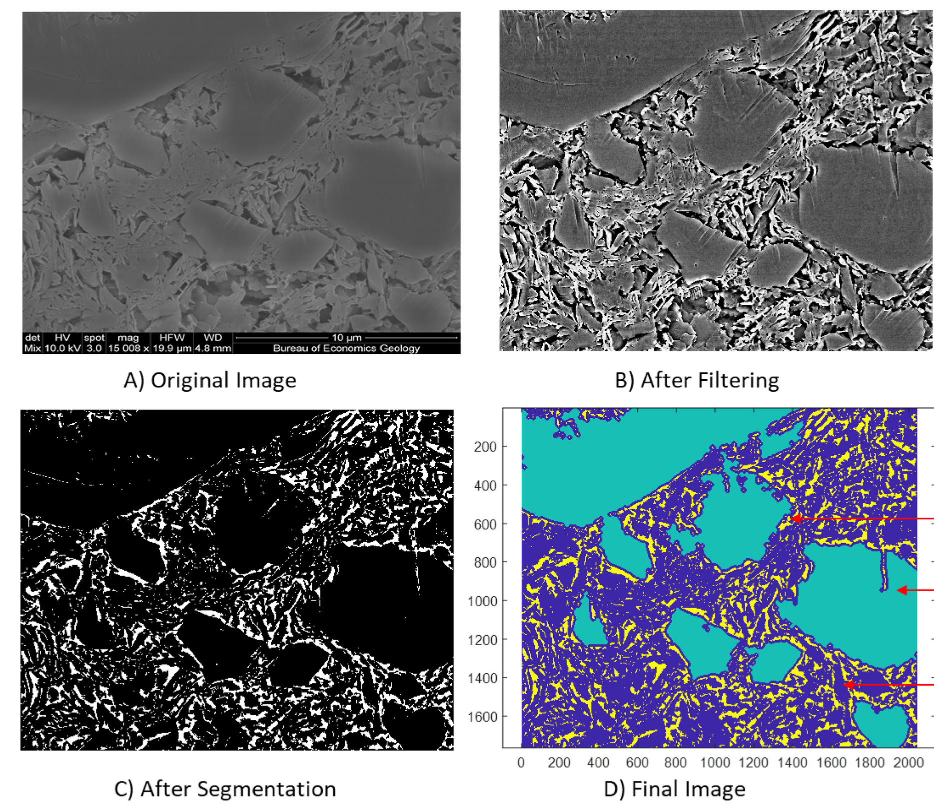

Figure 4 – Stages of filtering and segmentation. A) Original image, B) Image after median and top hat and bottom hat filtering, C) After binary segmentation, D) Final image with pores (yellow), silt size grains (cyan) and clay size grains (blue).

Segmentation from deep learning

- We created an alternative method for filtering and segmentation using deep learning to identify pore and grain features from SEM images to make the process more streamlined and easier to use.
- The trained model is available at: https://github.com/abhishekdbihani/deeplabV3_pores-grains

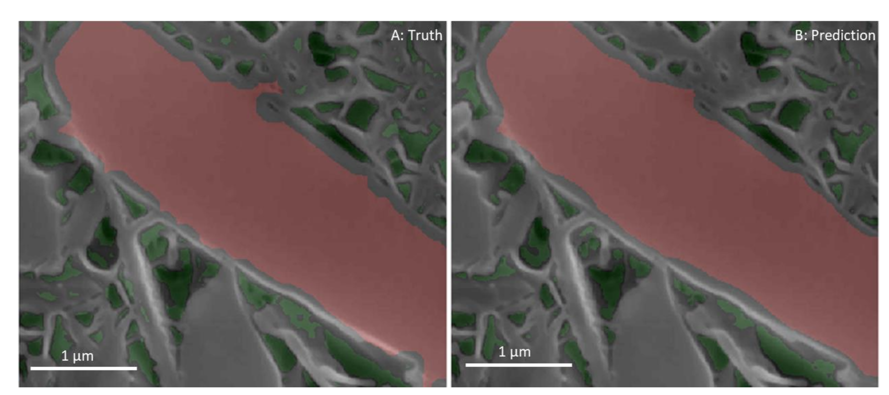

Figure 5 – Example of SEM image of silt grains (red) and pores (green): A) ground truth data, B) prediction from model

Grain-pore characteristics

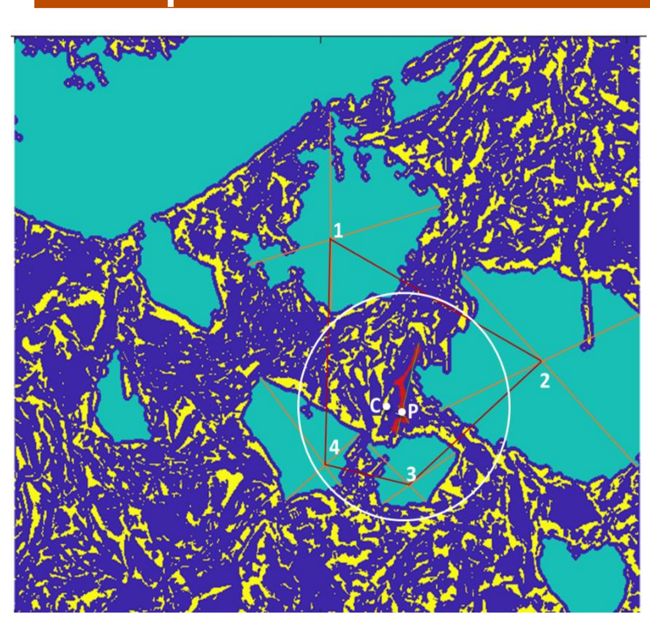

- The silt grains surrounding a pore (P) were determined, and the mean area of proximal silt grains was calculated.
- Centroid pore center distance: Centroid of polygon formed by the proximal grains was found (C) and the distance to the center of selected pore (C-P) was calculated.
- Mean proximal grain to pore distance: Mean of the distance from pore to the proximal grains was calculated.

Figure 6- Example of pore (red) with proximal silt grains 1, 2, 3, 4 (cyan) forming a polygon. P - pore center, C - centroid of proximal silt grains, white circle - mean of distance from P to proximal grain centers

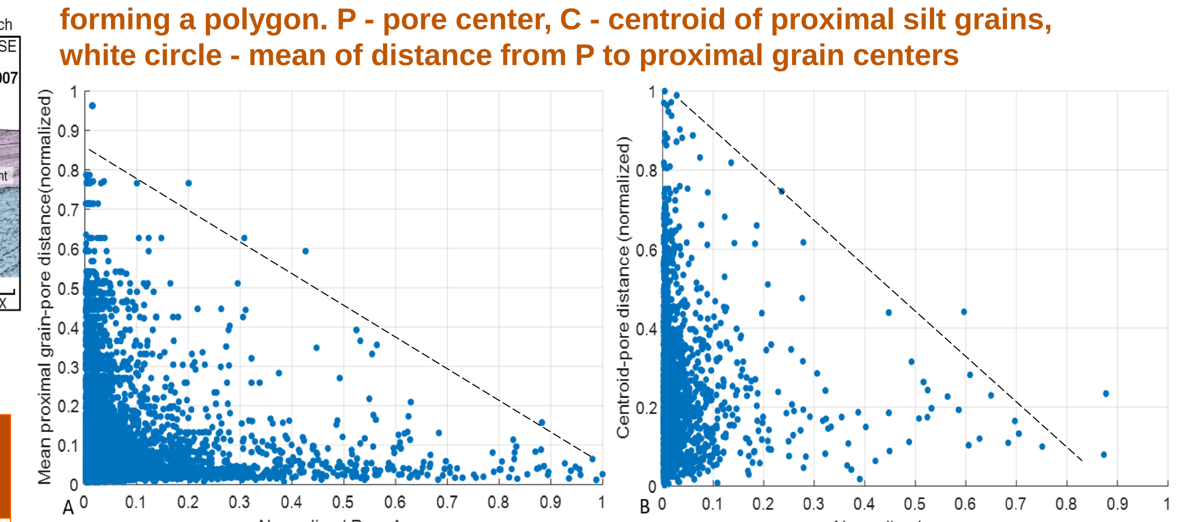

Figure 7 – Grain-pore characteristic plots: A) Mean proximal grain to pore distance and pore area, B) Centroid to pore center distance and pore area. (Black dashed line illustrates the envelope of the trend).

- Centroid to pore center distance and mean proximal grain to pore distance decreases with increasing pore area which suggests influence of silt bridging.

Silt content and porosity analysis for Site C0002

- Silt content from SEM images matches the trend from grain size analysis
- The visible porosity for depths of SEM images was calculated

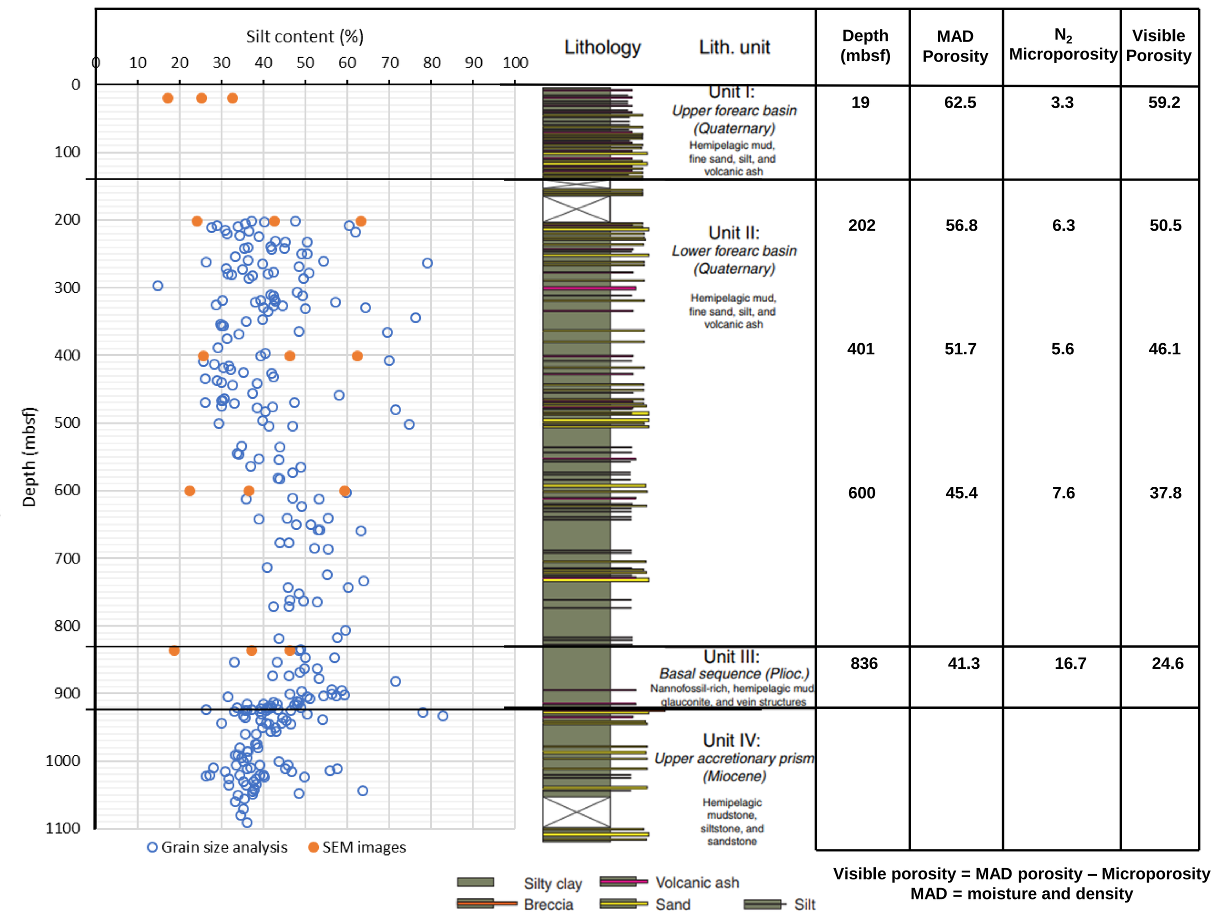

Figure 8 - Silt fraction comparison from SEM images (orange) and grain size analysis (blue), along with porosity values. (Modified from Moore et al., 2012 with data from Kopf et al., 2017 and Nole et al., 2016)

Grain pack creation

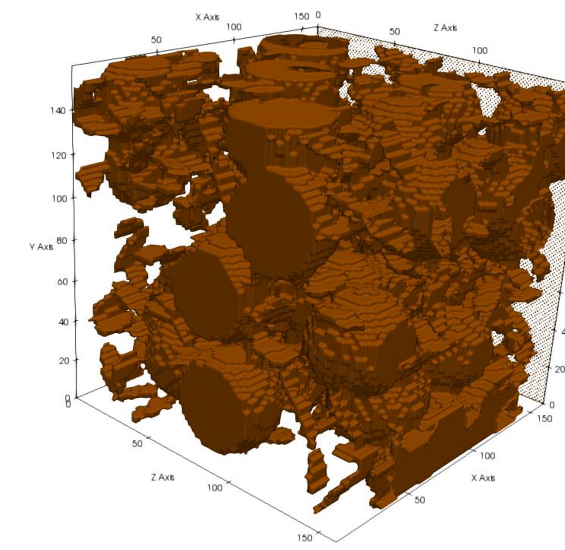

- Grain packs representing mudrocks were created from a stochastic process like Landry et al. (2017), with spherical silt grain and ellipsoidal clay grains.
- Two grain packs were created for each depth using the value of visible porosity.
- The fraction of spherical grains at a depth was varied using minimum and maximum silt content from the SEM images for investigating silt bridging.

Figure 9- An example grain pack with spherical and ellipsoidal grains (brown)

Lattice Boltzmann simulations

- A workflow was created for conducting LBM simulations using PALABOS library to calculate capillary pressure, permeability and tortuosity in the grain packs.
- The workflow can be found at: https://github.com/je-santos/MultiphasePorousMediaPalabos.
- Simulations were run to investigate flow of a non-wetting fluid across the grain packs, similar to hydrocarbon or CO_2 across a mudrock seal
- Each simulation run had multiple pressure increments to study flow behavior and were run on the STAMPEDE2 supercomputer.

Drainage capillary pressure curves

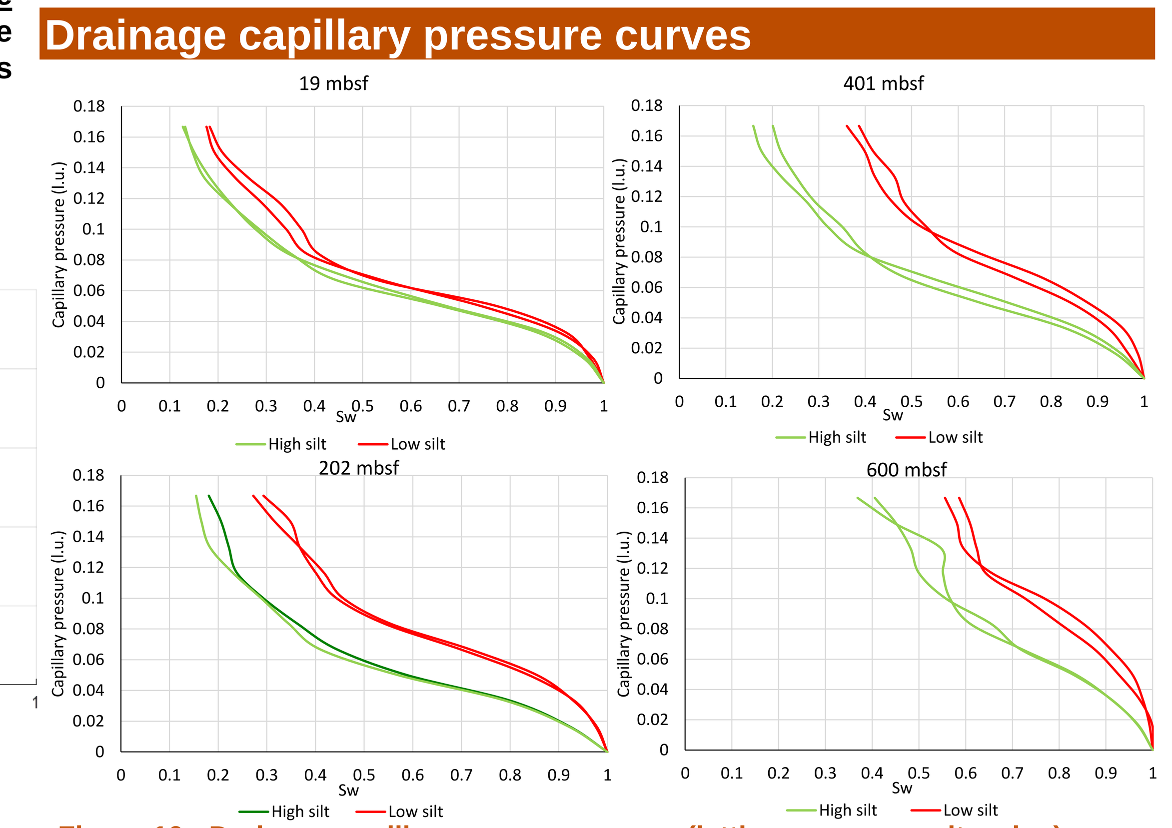

Figure 10 - Drainage capillary pressure curves (lattice pressure units – l.u.)

- With increasing depth, drainage P_c curves become steeper and have higher residual wetting phase saturations due to smaller pore throats
- At a given depth, with increasing silt content, capillary thresholds are observed at successively lower wetting saturations due to more larger throats

Flow path visualization

For dominant clay grain fractions (Figure 11 A), percolation path of non-wetting fluid is highly tortuous (T =1.43), while for higher silt fractions (Figure 11 B), the path is shorter (T = 1.12).

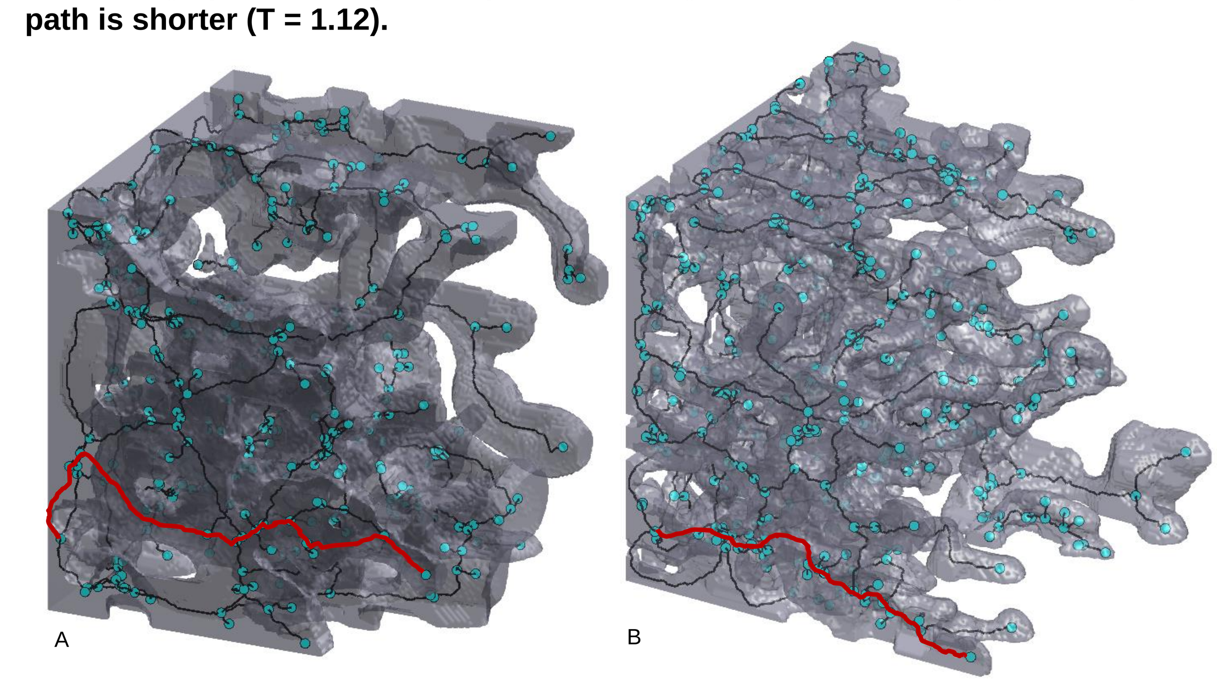

Figure 11 – Flow visualization of the non-wetting fluid in the grain packs at 401 mbsf: A) Minimum silt content (23.7 %), B) Maximum silt content (57.1 %). The flow paths are in black, with first path (percolation path) across the grain pack shown in red

Porosity and Absolute permeability trend

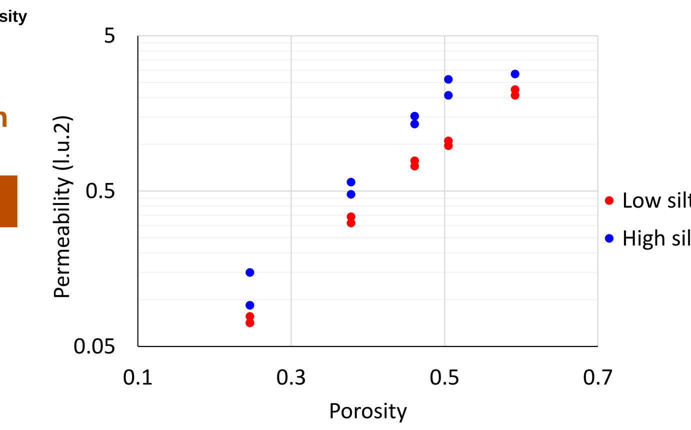

- Figure shows that porosity and absolute permeability both decrease with depth
- However, increasing silt content at a depth (with same porosity), increases the absolute permeability
- Increase in permeability at higher silt concentrations could be due to preserved larger pores due to silt-bridging effect

Figure 12 - Porosity and Absolute permeability of grain packs

Representative elementary volume check

- REV was checked by calculating the porosity and standard deviation of cubic subsamples at various length scales in increasing order.
- Porosity tapers towards mean and standard deviation decreases with length.

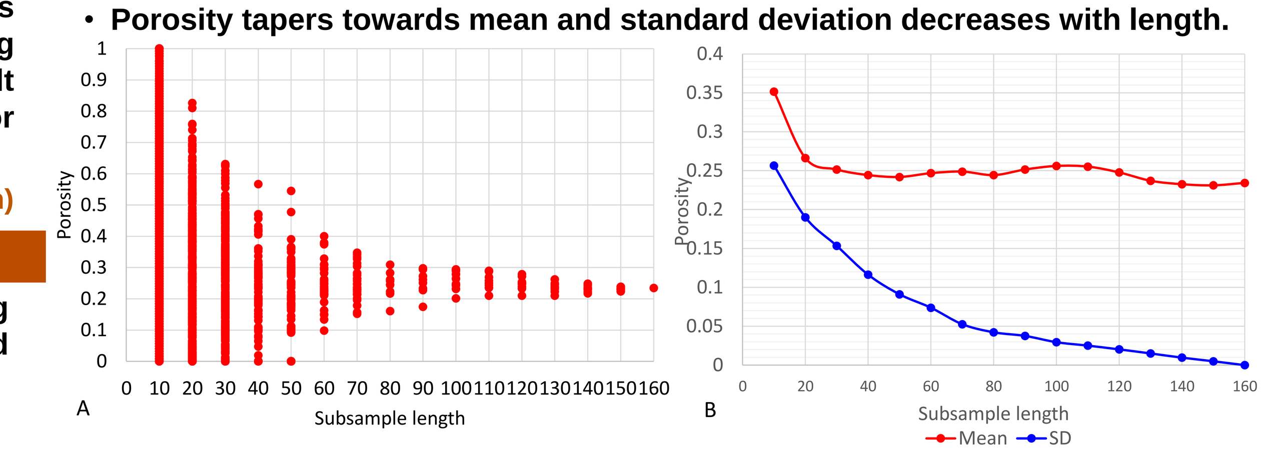

Figure 13- REV check of a sample grain pack: A) Porosity vs length; B) Mean porosity and Standard deviation of porosity vs length.

Conclusion

- Statistical analysis of the images showed that while the porosity decreased with increasing depth, larger pores were preserved when surrounded by larger grains, confirming the influence of the silt-bridging effect.
- LBM simulation results showed that at a depth, with increasing silt content, capillary pressures and tortuosity values decreased, while absolute permeabilities increased.
- Adequate characterization of a mudrock seal is necessary as silt bridging can cause seal failure even below the fracture pressure and allow trapped hydrocarbons or CO_2 below a mudrock seal to escape.

References

Bihani, A., & Daigle, H. (2019). On the role of spatially correlated heterogeneity in determining mudrock sealing capacity for CO2 sequestration. Marine and Petroleum Geology, 106(106), 116–127. https://doi.org/10.1016/j.marpetgeo.2019.04.038

Kopf, A., Strasser, M., Monsees, N., Underwood, M. B., & Guo, J. (2011). Data report : particle size analysis of sediments recovered during IODP Expeditions 315 and 316 , Sites C0001 – C0008 , Nankai Trough forearc , off Japan 1, 314(1914). https://doi.org/10.2204/iodp.proc.314315316.207.2011

Landry, C. J., Prodanović, M., Reed, R., Eichhubl, P., & Mohanty, K. (2017). Estimating Oil-Water Relative Permeability Curves Using Digital Rock Physics, URTeC, 24–26. http://doi.org/10.15530/urtec-2017-2691701

Milliken, K., Prodanovic, M., Nole, M., & Daigle, H. (2016, April 7). Unconsolidated muds from the Nankai Trough. Retrieved September 27, 2019, from https://www.digitalrocksportal.org/projects/42

Moore, G. F., Kanagawa, K., & Strasser, M. (2013). Expedition 338 Preliminary Report NanTroSEIZE Stage 3 : NanTroSEIZE plate boundary deep riser 2 1 October 2012 – 13 January 2013, (October 2012). http://doi.org/10.2204/iodp.pr.338.2013

Nole, M., Daigle, H., Milliken, K. L., & Prodanović, M. (2016). A method for estimating microporosity of fine-grained sediments and sedimentary rocks via scanning electron microscope image analysis. Sedimentology, 63, 1507–1521. http://doi.org/10.1111/sed.12271

Schneider, J., Flemings, P. B., Day-Stirrat, R. J., & Germaine, J. T. (2011). Insights into pore-scale controls on mudstone permeability through resedimentation experiments. Geology, 39(11), 1011–1014.

Acknowledgements

The authors would like to thank University of Texas at Austin for the support, TACC for providing computational services, and Equinor for funding this research through the Statoil Fellows program. Samples and data were provided by the Integrated Ocean Drilling Program (IODP).

Contact: abihani@utexas.edu